RESEARCH ARTICLE

CME

Glia Imaging Differentiates Multiple System Atrophy from Parkinson's Disease: A Positron Emission Tomography Study with [^{11}C]PBR28 and Machine Learning Analysis

Aurelija Jucaite, MD, PhD,[1,2*] Zsolt Cselényi, MD, PhD,[1,2] William C. Kreisl, MD,[3] Eugenii A. Rabiner, MD,[4,5] Andrea Varrone, MD, PhD,[2] Richard E. Carson, PhD,[6] Juha O. Rinne, MD, PhD,[7] Alicia Savage,[8] Magnus Schou, PhD,[1,2] Peter Johnström, PhD,[1,2] Per Svenningsson, MD, PhD,[9] Olivier Rascol, MD, PhD,[10] Wassilios G. Meissner, MD, PhD,[11,12,13] Paolo Barone, MD, PhD,[14] Klaus Seppi, MD,[15] Horacio Kaufmann, MD, PhD,[16] Gregor K. Wenning, MD, PhD, MSc,[17] Werner Poewe, MD,[17] and Lars Farde, MD, PhD[2]

[1]*PET Science Centre, Personalized Medicine and Biosamples, R&D, AstraZeneca, Stockholm, Sweden*
[2]*Department of Clinical Neuroscience, Centre for Psychiatry Research, Karolinska Institutet, Stockholm, Sweden*
[3]*Taub Institute, Department of Neurology, Columbia University Irving Medical Centre, New York, New York, USA*
[4]*Invicro, London, UK*
[5]*Centre for Neuroimaging Sciences, Institute of Psychiatry, Psychology and Neuroscience, King's College London, London, UK*
[6]*Yale University PET Centre, New Haven, Connecticut, USA*
[7]*Turku PET Centre, University of Turku and Turku University Hospital, Turku, Finland*
[8]*R&D, AstraZeneca, Waltham, Massachusetts, USA*
[9]*Section of Neurology, Department of Clinical Neuroscience, Karolinska Institutet, Stockholm, Sweden*
[10]*French MSA Reference Centre, Clinical Investigation Centre CIC1436, Department of Neurosciences and Clinical Pharmacology, NeuroToul COEN Centre, UMR 1 214-ToNIC and University Hospital of Toulouse, INSERM and University of Toulouse 3, Toulouse, France*
[11]*CRMR AMS, Service de Neurologie-Maladies Neurodégénératives, CHU Bordeaux, Bordeaux, France*
[12]*University Bordeaux, CNRS, IMN, UMR 5293, Bordeaux, France*
[13]*Department of Medicine, University of Otago, Christchurch, New Zealand Brain Research Institute, Christchurch, New Zealand*
[14]*Neurodegenerative Disease Centre, University of Salerno, Salerno, Italy*
[15]*Department of Neurology, Innsbruck Medical University, Innsbruck, Austria*
[16]*Department of Medicine, NYU Grossman School of Medicine, New York, New York, USA*
[17]*Division of Clinical Neurobiology, Department of Neurology, Innsbruck Medical University, Innsbruck, Austria*

ABSTRACT: Background: The clinical diagnosis of multiple system atrophy (MSA) is challenged by overlapping features with Parkinson's disease (PD) and late-onset ataxias. Additional biomarkers are needed to confirm MSA and to advance the understanding of pathophysiology. Positron emission tomography (PET) imaging of the translocator protein (TSPO), expressed by glia cells, has shown elevations in MSA.
Objective: In this multicenter PET study, we assess the performance of TSPO imaging as a diagnostic marker for MSA.
Methods: We analyzed [^{11}C]PBR28 binding to TSPO using imaging data of 66 patients with MSA and 24 patients with PD. Group comparisons were based on regional analysis of parametric images. The diagnostic readout included visual reading of PET images against clinical diagnosis and machine learning analyses. Sensitivity, specificity, and receiver operating curves were used to discriminate MSA from PD and cerebellar from parkinsonian variant MSA.
Results: We observed a conspicuous pattern of elevated regional [^{11}C]PBR28 binding to TSPO in MSA as

*__Correspondence to:__ Dr. Aurelija Jucaite, AstraZeneca, R&D, Department of Clinical Neuroscience, R5:02, Karolinska University Hospital, SE-17176 Stockholm, Sweden; E-mail: aurelija.jucaite@astrazeneca.com

Aurelija Jucaite and Zsolt Cselényi are cofirst authors.

Relevant conflicts of interest/financial disclosures: A.J., Z.C., P.J., M.S., A.S., and L.F. were full-time employees of AstraZeneca at the time the study was conducted and during manuscript preparation. W.G.M. has received fees from AstraZeneca as an advisory board member. A.V., W.C.K., J.O.R., E.A.R., R.E.C., O.R., W.G.M., P.B., K.S., H.K., G.K.W., and W.P. declare no conflict of interest.

Full financial disclosures and author roles may be found in the online version of this article.

Received: 4 May 2021; **Revised:** 6 September 2021; **Accepted:** 10 September 2021

Published online 5 October 2021 in Wiley Online Library (wileyonlinelibrary.com). DOI: 10.1002/mds.28814

compared with PD, with "hotspots" in the lentiform nucleus and cerebellar white matter. Visual reading discriminated MSA from PD with 100% specificity and 83% sensitivity. The machine learning approach improved sensitivity to 96%. We identified MSA subtype-specific TSPO binding patterns.

Conclusions: We found a pattern of significantly increased regional glial TSPO binding in patients with MSA. Intriguingly, our data are in line with severe neuroinflammation in MSA. Glia imaging may have potential to support clinical MSA diagnosis and patient stratification in clinical trials on novel drug therapies for an α-synucleinopathy that remains strikingly incurable.

Key Words: multiple system atrophy; microglia; translocator protein; positron emission tomography; [^{11}C] PBR28

Multiple system atrophy (MSA) is a rare fatal neurological disorder of unknown etiology. The clinical picture is characterized by motor and autonomic dysfunction. Based on the motor presentation, MSA is divided into a parkinsonian (MSA-P) and a cerebellar variant (MSA-C).[1] A major clinical challenge is the differentiation between MSA-P and PD or between MSA-C and idiopathic late-onset cerebellar ataxia.[2] Although current clinical diagnostic criteria perform well in later disease stages, sensitivity has been reported to reach only about 30% at first examination, and a definite MSA diagnosis is still anchored on postmortem examination.[3-6] Hence the development of sensitive biomarkers for early diagnosis is an important medical need, and in particular with respect to patient recruitment for disease modification trials.

The neuropathology of MSA is characterized by glial and neuronal cytoplasmic inclusions containing misfolded α-synuclein (αSYN) leading in particular to a prominent neuronal loss in nigrostriatal and olivopontocerebellar brain structures.[7] The progression of MSA pathology is accompanied by neuroinflammation, presenting with elevated levels of proinflammatory cytokines[8] and widespread microgliosis.[9,10] A glia response in vivo has been reported in a small group of patients with MSA, using positron emission tomography (PET) imaging of the translocator protein (TSPO), a marker for microglia and astrocytes.[11,12] Therefore, it is plausible that TSPO imaging could provide additional information on MSA pathophysiology and have potential for diagnostic purposes.

In this analysis, we examined the diagnostic sensitivity and specificity of TSPO imaging for discrimination of MSA and PD and between MSA subtypes. Besides visual reading, a machine learning (ML) approach was applied to obtain a glia imaging signature of MSA.

Subjects and Methods

Participants and image analysis methodology are briefly presented later. For detailed information, see Supporting Information Appendix 1.

Participants

Two groups of patients were included who had participated in two separate multicenter phase 2a clinical trials with the myeloperoxidase inhibitor, verdiperstat (AZD3241, BHV-3241): (1) the group of patients with MSA (ClinicalTrials.gov: NCT02388295; the first patient was enrolled on April 27, 2015, and the last patient last visit was September 29, 2016), and (2) a comparator group of previously examined patients with PD (EudraCT Number: 2011-004803-19; ClinicalTrials.gov: NCT01527695, published in 2015; the first patient was enrolled on April 17, 2012, and the last patient's last visit was January 9, 2013; this study was reported by Jucaite et al.[13]). For both studies, only PET examinations acquired at screening (baseline) were included in this analysis.

The multicenter PET study in patients with MSA was approved by the local Research Ethics and Radiation Safety Committees and the Medical Products Agencies of participating countries in Europe and the United States (for a list of participating centers, see Supporting Information Appendix 1, pp. 3–4) and was performed in accordance with the current amendment of the Declaration of Helsinki and International Conference on Harmonization/Good Clinical Practice guidelines. Written informed consent was obtained from all study participants. Patients who fulfilled criteria for probable or possible MSA[1] were recruited by movement disorder specialists, and the diagnosis was confirmed centrally by independent reviewers (G.K.W. and H.K.). The diagnosis of MSA was supported by a qualitative magnetic resonance imaging (MRI) examination. The main inclusion criteria were stable on medical MSA treatment for 30 days before screening and during screening and patients defined as "high or mixed affinity binders"[14] with respect to [^{11}C]PBR28 binding to TSPO. Exclusion criteria were anatomical brain abnormalities detected on MRI other than typical for MSA, any significant other neurological or psychiatric disease, major or unstable somatic disease, and "low-affinity binders" to TSPO. For more details on inclusion/exclusion criteria in the PD group, see Appendix S1, Supplementary Methods and Jucaite et al.[13]

Procedures

Clinical Assessments

MSA symptom severity was assessed using the Unified Multiple System Atrophy Rating Scale (UMSARS),[15] and the autonomic nervous system was examined using the Composite Autonomic Symptom Scale. Safety assessments included records of adverse events, vital signs, electrocardiogram, clinical chemistry, hematology, and urine analysis. Patients with PD had been assessed for disease severity and motor signs using the Unified Parkinson's Disease Rating Scale (UPDRS).[16] Demographic data from both patient groups are presented in Table 1.

Genotyping for TSPO Polymorphisms

Genotyping for single-nucleotide polymorphism of TSPO (DNA polymorphism rs6971, Ala substitution by Thr at 147 amino acid position) was performed prospectively at each of the participating clinical centers and was used to exclude low-affinity binders.[14]

Safety Assessments

Safety and tolerability assessments included records of adverse events, vital signs (pulse, blood pressure), electrocardiogram, clinical chemistry and hematology assessments, and urinalysis.

TABLE 1 *Demographic and disease characteristics*

Patient characteristics	MSA group (n = 66)	PD group (n = 24)
Age, mean ± SD, y (range)	59 ± 7 (43–74)	62 ± 6 (50–73)
Sex (female/male), n	46/20	21/3
MSA diagnostic type (MSA-P/MSA-C), n	30/36	NA
MSA category (possible/probable), n	17/49	NA
UMSARS total score (at screen),[a] mean ± SD (range)	46 ± 12 (23–77)	NA
UMSARS Part II motor score (at screen),[a] mean ± SD (range)	24 ± 7 (12–43)	NA
UPDRS score, mean ± SD (range)	NA	25 ± 6 (6–29)
TSPO genotype (MAB/HAB), n	23/43	13/11

[a]UMSARS score data are available for participants who completed the trial (n = 53).
MSA, multiple system atrophy; PD, Parkinson's disease; SD, standard deviation; MSA-P, parkinsonian subtype MSA; MSA-C, cerebellar subtype MSA; UMSARS, Unified Multiple System Atrophy Rating Scale; UPDRS, Unified Parkinson's Disease Rating Scale; TSPO, translocator protein; MAB, mixed affinity binder; HAB, high-affinity binder; NA, not applicable.

Imaging Data Acquisition

Imaging data acquisition and quality control were guided by the MR and PET Imaging Procedure Manuals, prepared and monitored by BioClinica Inc. (Newark, CA, USA). Brain MRI were acquired at 16 participating clinical centers using center-specific protocols. MRI examinations using a T1-weighted sequence were used as anatomical reference for PET image analysis. Other sequences included T2-weighted, fluid-attenuated inversion recovery (FLAIR), diffusion-weighted imaging (Supporting Information Appendix 1, p. 5) and served for the diagnosis of MSA, using MRI as "additional criteria."[1]

PET data were acquired at five PET centers, satisfying radiation safety requirements in each country and using a common protocol adjusted to local routines (Supporting Information Appendix 1, p. 5). [^{11}C]PBR28 was prepared from its corresponding desmethyl-PBR28 precursor.[17] Quality-control and radioligand release criteria were implemented to assure uniform quality of [^{11}C]PBR28. The radioactivity, molar activity, and mass of [^{11}C]PBR28 administered intravenously at each PET center are presented in Supporting Information Table 1 in Appendix 1.

The protocol included arterial blood sampling and analysis of radioligand metabolites in plasma to be used in the quantitative image analysis. Analysis of blood and plasma radioactivity concentrations and measurements of [^{11}C]PBR28 metabolites were performed at PET centers independently according to a common protocol adjusted to local routines. Importantly, at all imaging centers, time curves of radioactivity concentration in whole blood and total plasma, as well as of the fraction of unchanged [^{11}C]PBR28, were acquired during the PET measurement. The time curves and all imaging data were then transferred to AstraZeneca PET Science Center at Karolinska Institutet (Stockholm, Sweden) for central processing.

For PET data acquisition details in the PD patient group, see Appendix S1, Supplementary Methods and Jucaite et al.[13]

Image Processing

The T1-weighted MRIs were reoriented, resampled, and cropped to generate a 220 × 220 × 170 matrix with 1-mm^3 voxels. These MRIs were segmented into gray matter, white matter, and cerebrospinal fluid and warped the individual image into the Montreal Neurological Institute template space using the SPM12 software (Wellcome Department of Cognitive Neurology, London, UK). The brain regions of interest (ROIs) were obtained using the automatic anatomical labeling template[18] and modification for subcortical structures.[19] The list of 39 ROIs included regions of the nigrostriatal system, lentiform nucleus (pooling

putamen and pallidum) and cerebral cortex subregions, thalamus, whole cerebellum, cerebellar white matter, subcortical white matter, whole white matter, gray matter, and whole brain (by summing the gray and white matter segments). Furthermore, the two regions of so-called hotspots were also defined using the inter-individual median binding images for patients with MSA: a region containing the highest binding within lentiform nucleus (using the median image for patients with MSA-P) and, separately, cerebellar white matter (using the median image for patients with MSA-C) with binding reaching 90% or higher of the peak value within each anatomical area. Thus, in total, 41 ROI definitions were obtained.

The arterial blood processing and generation of arterial input function is described in Supporting Information Appendix 1.

Image Analysis

Quantification of [^{11}C]PBR28 Binding and Group Comparisons

[^{11}C]PBR28 binding to TSPO in brain was quantified by using the multilinear version of Logan's graphical analysis and wavelet aided parametric imaging to obtain values for the total distribution volume (V_T) for each volume element (voxel).[20] Regional V_T values were obtained by applying 39 brain anatomical ROIs from automatic anatomical labeling atlas[14] to the parametric images and calculating the mean voxel value for each ROI. Two additional regions were added after qualitative evaluation of the V_T images. These regions corresponded to areas of increased tracer uptake, are referred to as "hotspots" at the level of the lentiform nucleus and cerebellar white matter, and were operationally defined as including voxels with V_T values ≥90% of the peak regional value in patients with MSA.

The global effect of clinical diagnosis (PD, MSA, MSA-P, and MSA-C) on the whole-brain V_T was evaluated using a linear mixed effects model accounting for possible confounders (the fixed effects of age, sex, and TSPO genotype, random effect of the imaging site).[21] Subsequently, the association between clinical diagnosis and regional TSPO binding was assessed using a simplified model retaining only the main effect of clinical diagnosis and the nuisance effect of TSPO genotype as the only relevant confounder based on the global fit.

Brain Images for Visual Reading and Pattern Analysis by Machine Learning

To obtain a static image of sufficient quality for visual reading, we summed radioactivity acquired from 30 to 66 minutes after injection.[13] For ML, the individual summation PET images were divided by the whole-brain average radioactivity value to obtain normalized standardized uptake value (nSUV) images. In a similar manner, individual V_T parametric images were normalized to (ie, divided by) the whole-brain V_T value to obtain nV_T images. The nSUV and nV_T images were warped to the Montreal Neurology Institute template space for ML and also to derive group-wise, median images for reader training.

Classification

Visual Reading

Three PET researchers at Karolinska Institutet who were not involved in the study and blinded to the clinical diagnosis read the late summation radioactivity image and assigned a diagnostic label (PD, MSA-P, or MSA-C) for each patient. Furthermore, in case of an MSA-P or MSA-C label, the reader could indicate the presence of a mixed pattern of [^{11}C]PBR28 distribution if there was a visually similar signal both for lentiform nucleus and for cerebellar white matter. For further details, description of the software package, along with guidelines, training, and test images, see Supporting Information Appendix 1.

Machine Learning

Either nSUV or nV_T parametric images were used as input to enable automatic image-based assessment of the clinical diagnosis. A cross-validated multivariate linear-discriminant classifier (LDC) was obtained.[22] The LDC regression step provided three sets of regression coefficients corresponding to the linear boundaries between each pair of classes: MSA-P versus PD, MSA-C versus PD, and MSA-C versus MSA-P. The regression coefficients were used to obtain three brain scores for each subject corresponding to each of the decision boundaries, respectively. The brain scores were converted to posterior probabilities of belonging to each class among all possible classes. Finally, the class with the highest probability was assigned as the label for each subject. For the purpose of visualizing the resulting brain scores, the MSA-P versus PD and MSA-C versus PD decision boundaries were "collapsed" to obtain an overall score for the MSA versus PD differentiation.

The LDC algorithm was used in two steps. First, a full model (including data from all subjects) was used to obtain fitted scores and classification readouts for all subjects. The full model results were used for visualization of brain scores. Then predicted, cross-validated scores and classification readouts were obtained for each subject using a leave-one-out cross-validation approach. In other words, for each subject, the prediction was made using a reduced LDC model excluding that subject. This step allowed us to determine the diagnostic performance of the ML approach.

Statistical Analysis

All statistical analyses were performed and LDC implemented by using the Statistics and Machine Learning Toolbox in MATLAB (MathWorks, 2014). Linear fixed effect models with control of false discovery rate[23] were used for group comparisons.

In the ML analysis, receiver operating curves (ROCs) were obtained to calculate the area under the curve (AUC) as a measure of classification performance.

Results

In total, 124 patients with MSA were screened, and 61 patients were randomized and entered into the clinical trial (Supporting Information Fig. 1 in Appendix 1). The main reasons for failure at screening (before and after PET examination) were withdrawn consent, respiratory and urinary tract infection, hepatitis C, laboratory values outside the limits for inclusion, prohibited concomitant medications, low-affinity binders for TSPO, and inability to comply with study procedures in time.

During the screening period, 66 patients with MSA, 47 male and 19 female patients aged 43–74 years, underwent a PET examination with [^{11}C]PBR28 after confirmation of TSPO genotype (high-affinity and mixed affinity binding). The UMSARS II score (motor examination) ranged from 12 to 43 (Table 1).

The comparison group consisted of 24 patients with PD, 21 male and 3 female patients, aged 50–73 years, with a Unified Parkinson's Disease Rating Scale Part III score (motor examination) ranging from 6 to 29 (Table 1). Details on patient selection and the clinical trial have been reported previously.[13]

[^{11}C]PBR28 Binding to TSPO and Group Comparisons

Visual inspection of PET images of patients with MSA revealed consistent hotspots of elevated [^{11}C]PBR28 binding in the lentiform nucleus or cerebellar white matter, whereas no such hotspots were seen in PD (Fig. 1A, aside of hotspots, note high [^{11}C]PBR28 binding in cerebellar peduncles and pons).

First, we compared whole-brain V_T values between the MSA and PD patient groups, including assessment of potential confounders, among which only TSPO genotype had a significant effect on [^{11}C]PBR28 binding (Supporting Information Table 2 in Appendix 1).

Thereafter, we compared patient groups and accounting for the genotype effect, we found significantly higher V_T in lentiform nucleus, cerebellar white matter, and subcortical white matter (centrum semiovale) in the MSA group (Table 2). With regard to MSA subtypes, the statistically significant and largest effect on binding was detected in the lentiform nucleus in MSA-P compared with PD and in the cerebellar white matter in MSA-C

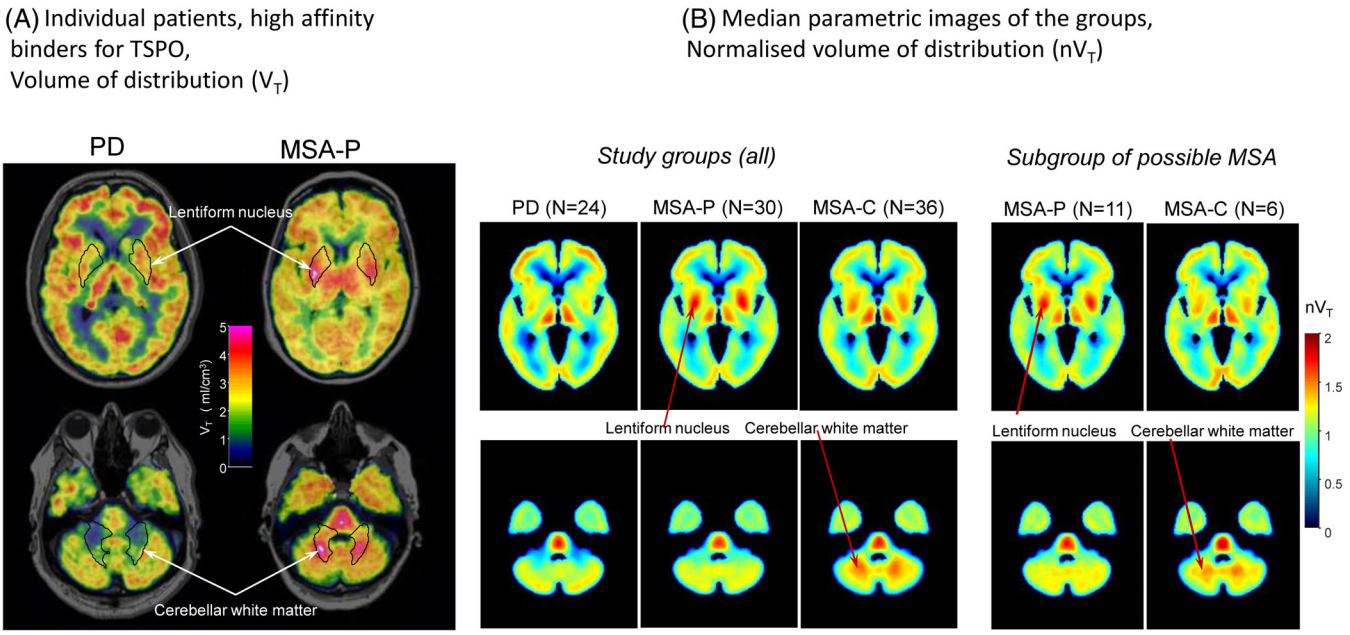

FIG. 1. (**A**) Parametric images of total volume of distribution (V_T) of [^{11}C]PBR28 in a patient with Parkinson's disease (PD) and with multiple system atrophy (MSA). Contours show region of interest definitions obtained from the automatic anatomical labeling template. Aside of "hotspots" in the lentiform nucleus and cerebellar white matter there is high [^{11}C]PBR28 binding to translocator protein (TSPO) in cerebellar peduncles and pons. Although clinically assigned to predominantly MSA-P, this patient is representative of so-called mixed MSA. (**B**) Median parametric images of total normalized [^{11}C]PBR28 binding for PD and MSA patient groups. PET images map regional total volume of distribution normalized to the whole brain (nV_T). Each voxel represents the interindividual median for patients with PD, parkinsonian type MSA (MSA-P), and cerebellar type MSA (MSA-C), respectively. [Color figure can be viewed at wileyonlinelibrary.com]

TABLE 2 *Group comparison of regional binding of [^{11}C]PBR28 (V_T) in brain regions with significant difference between MSA and PD*

Region of interest	Estimate: β (SE)	*t*-statistic	*P* value	95% CI	FDR-adjusted *P* value (q = 0.05)	FCR-adjusted CI
White matter						
Cerebellar white matter (anatomical)	0.951 (0.220)	4.314	4.21×10^{-5}	0.513–1.389	0.002	0.331–1.570
"Hotspot" in cerebellar white matter	0.906 (0.263)	3.441	8.93×10^{-4}	0.383–1.430	0.016	0.166–1.647
Subcortical white matter (centrum semiovale)	0.346 (0.113)	3.061	0.003	0.121–0.571	0.030	0.028–0.664
Gray matter						
Basal ganglia	0.401 (0.193)	2.082	0.040	0.018–0.784	0.165	N/A
Dorsal striatum (caudate/putamen)	0.426 (0.191)	2.231	0.028	0.047–0.805	0.143	N/A
Lentiform nucleus (putamen/pallidum)	0.595 (0.219)	2.715	0.008	0.160–1.031	0.055	N/A
Putamen	0.577 (0.220)	2.616	0.010	0.139–1.015	0.061	N/A
Pallidum	0.654 (0.220)	2.973	0.004	0.217–1.092	0.031	0.036–1.273
"Hotspot" in lentiform nucleus	0.938 (0.280)	3.355	0.001	0.382–1.494	0.016	0.152–1.724
Parahippocampus	0.352 (0.175)	2.003	0.048	0.003–0.700	0.180	N/A
Substantia nigra	0.488 (0.223)	2.189	0.031	0.045–0.931	0.143	N/A

Explorative analysis using linear fixed effect model with two fixed effects: the main effect of clinical diagnosis (results shown) and the nuisance effect of translocator protein (TSPO) genotype (results not shown). For exploratory purposes, regions with significant difference before and after correction are presented. The region-specific *P* values for the main effect of clinical diagnosis were corrected for the false discovery rate (FDR = 0.05)[22] and the corresponding false coverage statement rate (FCR). Adjusted confidence intervals (CIs) were computed for regions having statistically significant corrected *P* values.
V_T, total distribution volume; MSA, multiple system atrophy; PD, Parkinson's disease; SE, standard error; N/A, not applicable.

versus PD (Supporting Information Table 3 and Fig. 6 in Appendix 1).

The lack of a global effect of clinical diagnosis supported the use of whole-brain normalization without the risk of affecting group differences, while allowing for suppression of any nuisance global effects such as that of the TSPO genotype. The group-wise, interindividual median nV_T parametric images were created and used for training of the visual readers and illustrate the differences in TSPO pattern between PD and MSA patient groups, as well as MSA subtypes (Fig. 1B).

When analyzing TSPO binding pattern, we asked whether it can be observed in patients with possible MSA, when diagnosis is most challenging. We generated median nV_T images for the subgroups of patients with possible MSA-P and MSA-C, and the characteristic TSPO binding pattern was present (Fig. 1B).

Visual Reading

The majority vote of visual reading of the late summation images of [^{11}C]PBR28 binding pattern against the clinical diagnosis by three readers had 100% specificity and 83% sensitivity in discriminating patients with MSA from those with PD, and slightly lower values in discriminating MSA-C from MSA-P (Table 3 and Supporting Information Fig. 2 in Appendix 1). There was a moderate to substantial agreement either as compared with the clinical diagnosis (Cohen's κ = 0.6–0.8) or between readers (Fleiss' κ = 0.76) that was statistically significant ($P < 0.00001$), that is, supporting the rejection of an accidental agreement.

Machine Learning

The LDC performed using nSUV images provided 100% specificity and 89% sensitivity in differentiating MSA from PD. The ML executed on nV_T images had 100% specificity and 96% sensitivity in differentiating MSA from PD (Table 3). Cohen's κ indicated substantial agreement with the clinical diagnosis (κ = 0.68–0.92) that was statistically significant ($P < 0.00001$) supporting nonaccidental agreement.

Note that visual readers tended to be more "cautious" than the ML approach in the recognition of MSA-C in contrast with MSA-P as indicated by the higher specificity and lower sensitivity. The reason behind this may be that the lentiform "hotspot" is easier to visually

TABLE 3 *Diagnostic readout performance for visual reading and machine learning*[a]

Disease conditions	Performance measure	Reader 1 (n = 81)	Reader 2 (n = 81)	Reader 3 (n = 81)	Majority (n = 81)	LDC, nSUV (n = 90)	LDC, nV_T (n = 90)
MSA vs. PD	Specificity	100%	95%	100%	100%	100%	100%
	Sensitivity	88%	77%	80%	83%	89%	96%
	Cohen's κ	0.80	0.60	0.67	0.72	0.82	0.92
	Interrater Fleiss's κ	0.76 (95% CI: 0.73–0.79)					
MSA-C vs. MSA-P	Specificity	91%	87%	96%	91%	81%	86%
	Sensitivity	77%	70%	64%	74%	91%	83%
	Cohen's κ	0.66	0.57	0.60	0.65	0.72	0.68
	Interrater Fleiss's κ	0.76 (95% CI: 0.71–0.80)					

Agreement against the clinical diagnosis assessed with Cohen's unweighted kappa (κ).[23] The interrater consistency for visual readers was assessed by calculating Fleiss's κ, set at the 5% significance level.[24,25]

Note that visual readers tended to be more "cautious" than the machine learning approach in the recognition of cerebellar type MSA (MSA-C) in contrast with parkinsonian type MSA (MSA-P) as indicated by the higher specificity and lower sensitivity. The reason behind this may be that the lentiform "hotspot" is easier to visually recognize and evaluate than the more diffuse cerebellar white matter involvement, biasing the comparison of the two toward the former. Machine learning, which uses weighted sums across all brain voxels, can thus provide a more balanced performance in this task.

[a]Readout performance was evaluated against clinical diagnosis.

LDC, linear discriminant classifier; nSUV, whole-brain normalized standardized uptake value; nV_T, whole-brain normalized total volume of distribution; MSA, multiple system atrophy; PD, Parkinson's disease; CI, confidence interval.

recognize and evaluate than the more diffuse cerebellar white matter involvement, biasing the comparison of the two toward the former. ML performance, which uses weighted sums across all brain voxels, thus provides a more balanced result.

A discriminant pattern of ML-derived brain scores confirms the highest weighted scores in lentiform nucleus and cerebellar white matter and also with elevated TSPO binding in subcortical white matter (Supporting Information Fig. 3 in Appendix 1). The fitted brain scores from the full LDC model were used to plot the results of visual reading and the two ML-based datasets (Fig. 2; also in detail in Supporting Information Fig. 5 in Appendix 1). The LDC cross-validated brain scores were used to visualize the effective ROC for ML (Supporting Information Fig. 4 in Appendix 1). The graphs show ROCs with high AUC (≥0.9) for any LDC model or disease comparison with almost ideal performance for the differential diagnosis of MSA as a whole versus PD and with AUCs close to 1.0.

Discussion

In this international multicenter PET imaging study in a large cohort of patients with MSA (n = 66), we discovered a distinct pattern of regional glia activity not reported in earlier studies.[11,12] Radioligand binding to the glia marker TSPO was significantly elevated in brain regions known to be involved in MSA pathology, that is, primarily in lentiform nucleus and cerebellar white matter. This regional TSPO pattern has potential clinical utility in differentiating MSA from PD.

The nature of elevated TSPO binding in MSA requires a more detailed understanding. An elevated density of activated microglia cells and astrocytes (both expressing TSPO), severe astrocytosis, in particular in the white matter, has been reported in MSA brains post mortem.[9,10,26-29] We hypothesize that the elevated region-specific TSPO pattern in vivo primarily represents an increase in the density of functionally diverse microglia cells and astrocytes across gray and white matter regions.

The different TSPO binding patterns in patients with MSA and PD may suggest different pathophysiology of those two synucleinopathies. Indeed, there are multiple elements of MSA pathophysiology that are in contrast with PD, for example, widespread myelin degeneration and oligodendrogliopathy,[30] differential α-syn strains and their cellular localization,[31] spread patterns, and overall substantially higher α-syn burden.[32] To further elucidate pathophysiology of MSA, molecular imaging could contribute with development of radioligands for mapping of astrocytes and different phenotypes of microglia.

The development of sensitive biomarkers for MSA is of critical importance to improve diagnostic accuracy in life, as well as for enrichment of clinical study populations during development of novel targeted drug therapies. Visual reading of unprocessed, static PET images gave reasonably good sensitivity, specificity, and moderate to substantial agreement with the clinical diagnosis, allowing for simpler, that is, static, image acquisition protocols.

In contrast with visual reading, the ML approach presented in this study relied on a simple whole-brain normalization of V_T (and SUV) images, which is

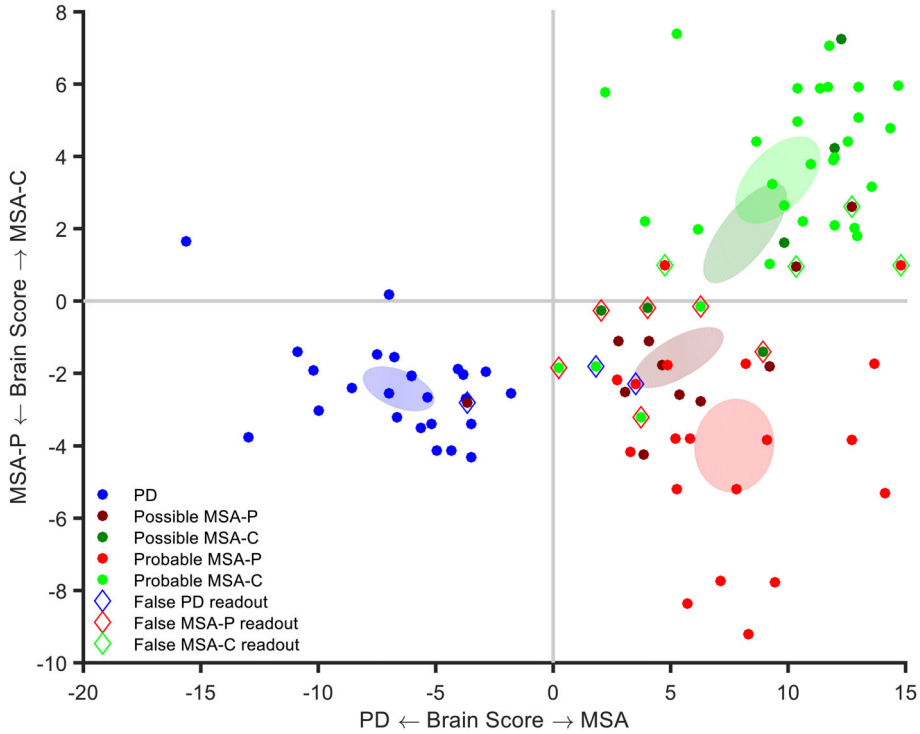

FIG. 2. Results of diagnostic readout obtained using cross-validated machine learning indicated on brain scores fitted according to the full machine learning model. x- and y-axis values indicate brain scores for differential diagnosis between multiple system atrophy (MSA) and Parkinson's disease (PD) and between cerebellar subtype of MSA (MSA-C) and parkinsonian subtype of MSA (MSA-P), respectively. Scatter points show fitted linear discriminant classification (LDC) scores with dot color according to the clinical diagnosis. Rhomboid markers indicate a false readout versus the clinical diagnosis with the marker color denoting the falsely predicted diagnosis. There is no extra marker in case of a correct diagnostic readout. Readout by cross-validated LDC based on nV_T parametric images; scatter points are for 90 patients from the full model. To illustrate typical patterns, the shaded ellipses indicate the locations of the top 10 percentile of bivariate Gaussian distributions fitted to the brain scores for the various patient populations. [Color figure can be viewed at wileyonlinelibrary.com]

comparable with, yet distinct from the use of a pseudo-reference region, such as the cerebellum in cases of Alzheimer's disease.[33] Importantly, this step was found to substantially diminish the influence of global effects on binding, such as TSPO genotype, sex, etc., and thus allowed for analysis of relative binding patterns in brain. In particular, the residual effect of genotype on normalized V_T values was estimated to be within typical test–retest variation for PET radioligand binding parameters (5–10%) (see Supporting Information Fig. 8).

The strength of this application of an ML approach is that the total binding pattern including even subtle regional differences is captured, such as TSPO elevation across white matter. Inclusion of all image information is a likely explanation for the excellent specificity and sensitivity obtained by machine reading. Worth noting is that the machine reading using simple nSUV images still had a significant classification performance. Accordingly, wider clinical use could incorporate machine reading based on static images, while expert centers or clinical research studies could benefit from using more extended acquisition protocols with arterial blood sampling to arrive at even more sensitive diagnostic readout using nV_T-based machine reading. This approach expands the utility of image-based automated classification analyses of metabolic, perfusion, presynaptic dopamine transporter (DAT) imaging, or different MRI methods, for example, volumetric or diffusion MRI used for the diagnosis of MSA.[34-38]

Current diagnostic criteria of possible MSA require the presence of one "additional feature," such as molecular imaging of DAT or glucose metabolism.[1] Whereas DAT loss is a feature of MSA-P, normal DAT availability does not exclude the diagnosis of MSA-C in the early stage of disease,[39] and glucose imaging in MSA diagnosis at disease onset also continues to be a challenge.[40] Our study suggests that glia imaging in MSA may be advantageous because even patients with possible MSA diagnosis or with relatively mild MSA (in this study, the UMSARS Part II motor scores ranged from 12 to 33) already have the specific pattern of regionally elevated TSPO levels that can be read with 100% specificity. Furthermore, TSPO was significantly elevated in white matter, which cannot be assessed by imaging of glucose metabolism or the dopaminergic system. Hence this study suggests that glia imaging has the potential to develop into an "additional biomarker" with clinical

utility for early MSA diagnosis because it provides a direct readout of the ongoing pathological process.

This study's data also allowed for comparison of TSPO binding between MSA subtypes. Interestingly, in the subset of patients with MSA with a strong dominance of the "hotspot" signal in either the lentiform nucleus or the cerebellar white matter, there was complete agreement between clinical diagnosis and classification. However, in about 23 patients (35%), the visual readers identified the TSPO pattern as "mixed" because of a similar signal in the two "hotspots" (Fig. 1A). Thus, our data confirm that despite dichotomy in predominant clinical symptoms, there is an underlying shared pathophysiology. This finding is also in line with a report on the graded widespread MSA pathology across clinical phenotypes.[41] Whether subtype division of MSA will remain significant in clinical diagnostics and emerging new treatment options is still unknown. Importantly, irrespective of regional predominance, the TSPO binding signal serves the purpose of differentiating MSA from PD as a potentially pathognomonic sign.

Further imaging of neuroinflammation in MSA using current and emerging radioligands is warranted. Neuroinflammation in vivo has been studied in a broad range of neurological disorders, and disease-specific topographic TSPO patterns have been reported.[42] Among them, the presently observed MSA-specific pattern is unique. Pilot examinations of other parkinsonian syndromes suggest that TSPO pattern in corticobasal degeneration and supranuclear palsy appears to be different,[43,44] although it should be reexamined using second generation TSPO radioligands. ■

Additional Comments and Limitations

A previously examined group of 24 patients with PD served as the comparison group, and no healthy subjects were included. The validity of this comparison is supported by three recent studies using the radioligand [^{11}C]PBR28 or [^{18}F] FEPPA and showing similar TSPO binding in patients with PD and control subjects.[45-47]

This study was an initial part of a clinical drug trial and not designed as a case–control study. Patients with uncertain diagnosis (PD vs. MSA) were thus not included. The present abnormal neuroinflammatory profile found in already diagnosed patients is a first step. The sensitivity and specificity of TSPO imaging should be further validated in a prospective study, including patients with parkinsonian syndrome and uncertain diagnosis.

The radioligand for TSPO imaging is of critical importance for the utility of its application in a clinical setting. The early studies in MSA using [^{11}C]PK11195, a first generation TSPO ligand, reported elevated TSPO in several brain regions.[11,12] However, the high nonspecific binding of [^{11}C]PK11195 likely precluded a more detailed analysis of the specific TSPO binding pattern, including white matter. The second generation radioligand [^{11}C]PBR28 has improved binding characteristics, but wider use is limited by the short half-life of carbon-11 (20.3 minutes). [^{11}C]PBR28 has to be synthesized on-site and cannot be shipped to other imaging centers. Of particular importance is the development of a suitable TSPO radioligand, which is insensitive to the rs6971 genotype. This would make it possible to examine the entire patient population, because at present low-affinity binders cannot benefit from TSPO imaging. Thus, for wider clinical applications of glia imaging, the availability of suitable ^{18}F-labeled radioligands insensitive to TSPO genotype is an identified need. To our knowledge, this need is currently being addressed.[48]

The glia imaging pattern may also vary with disease course. The imaging data presented originate from a clinical trial intended to examine drug effect on TSPO. As such, the study design and aims included no a priori question on associations between the regional TSPO binding and MSA symptoms or disease duration. The distinct TSPO pattern was an unexpected finding, which warrants prospective longitudinal TSPO investigations in MSA, potentially combined with αSYN imaging, to monitor disease progression and to elucidate a time-dependent role of glia involvement in MSA pathophysiology.

In summary, we found significantly increased glial TSPO binding in brain regions involved in MSA neuropathology. Our findings indicate that TSPO pattern discriminates MSA from PD with high specificity and sensitivity and may thus support the clinical diagnosis of MSA. Glia imaging in MSA may also serve for patient stratification in clinical trials on novel drug therapies, an unmet medical need for the treatment of MSA.

Acknowledgments: The studies were sponsored by AstraZeneca. We thank all participants and their families involved in this project for their cooperation. We thank clinical teams at the participating centers for patient recruitment (listed in Supporting Information Appendix 1). We thank the former project team at AstraZeneca (Cambridge, MA, USA) for valuable comments and discussions during the clinical trial design and study setup. We thank the members of the PET Centers for imaging data collection and primary workup, and Graham Searle and Göran Rosenqvist for challenging image reconstructions. We thank the Quintiles and Bioclinica teams for the study conduct and study operational procedures, and Irfan Qureshi (Biohaven, New Haven, CT, USA) for valuable comments on the manuscript.

Data Availability Statement

Software and visual reading guide are available on request. Processed image analysis data are available for use in collaborative studies to researchers upon reasonable request to the corresponding author. Access to de-identified participant data may be granted following review. Sharing of raw imaging data may be limited as

by policies of the respective data owners at time of request.

References

1. Gilman S, Wenning GK, Low PA, et al. Second consensus statement on the diagnosis of multiple system atrophy. Neurology 2008;71: 670–676.
2. Watanabe H, Riku Y, Hara K, et al. Clinical and imaging features of multiple system atrophy: challenges for an early and clinically definitive diagnosis. J Mov Disord 2018;11:107–120.
3. Fanciulli A, Wenning GK. Multiple-system atrophy. N Engl J Med 2015;372:249–263.
4. Stankovic I, Quinn N, Vignatelli L, et al. A critique of the second consensus criteria for multiple system atrophy. Mov Disord 2019; 34:975–984.
5. Koga S, Aoki N, Uitti RJ, et al. When DLB, PD, and PSP masquerade as MSA: an autopsy study of 134 patients. Neurology 2015;85: 404–412.
6. Osaki Y, Ben-Shlomo Y, Lees AJ, Wenning GK, Quinn NP. A validation exercise on the new consensus criteria for multiple system atrophy. Mov Disord 2009;24:2272–2276.
7. Meissner WG, Fernagut PO, Dehay B, et al. Multiple system atrophy: recent developments and future perspectives. Mov Disord 2019;34:1629–1642.
8. Yamasaki R, Yamaguchi H, Matsushita T, Fujii T, Hiwatashi A, Kira J-I. Early strong intrathecal inflammation in cerebellar type multiple system atrophy by cerebrospinal fluid cytokine/chemokine profiles: a case control study. J Neuroinflammation 2017;14:89.
9. Ishizawa K, Komori T, Sasaki S, Arai N, Mizutani T, Hirose T. Microglial activation parallels system degeneration in multiple system atrophy. J Neuropathol Exp Neurol 2004;63:43–52.
10. Salvesen L, Ullerup BH, Sunay FB, et al. Changes in total cell numbers of the basal ganglia in patients with multiple system atrophy - a stereological study. Neurobiol Dis 2015;74:104–113.
11. Gerhard A, Banati RB, Goerres GB, et al. [11C](R)-PK11195 PET imaging of microglial activation in multiple system atrophy. Neurology 2003;61:686–689.
12. Kübler D, Wächter T, Cabanel N, et al. Widespread microglial activation in multiple system atrophy. Mov Disord 2019;34:564–568.
13. Jucaite A, Svenningsson P, Rinne JO, et al. Effect of the myeloperoxidase inhibitor AZD3241 on microglia: a PET study in Parkinson's disease. Brain 2015;138(Pt 9):2687–2700.
14. Owen DR, Yeo AJ, Gunn RN, et al. An 18-kDa translocator protein (TSPO) polymorphism explains differences in binding affinity of the PET radioligand PBR28. J Cereb Blood Flow Metab 2012;32:1–5.
15. Wenning GK, Tison F, Seppi K, et al. Development and validation of the Unified Multiple System Atrophy Rating Scale (UMSARS). Mov Disord 2004;19:1391–1402.
16. Goetz CG, Fahn S, Martinez-Martin P, et al. Movement Disorder Society-sponsored revision of the unified Parkinson's disease rating scale (MDS-UPDRS): process, format, and clinimetric testing plan. Mov Disord 2007;22:41–47.
17. Briard E, Zoghbi SS, Imaizumi M, et al. Synthesis and evaluation in monkey of two sensitive 11C-labeled aryloxyanilide ligands for imaging brain peripheral benzodiazepine receptors in vivo. J Med Chem 2008;51:17–30.
18. Tzourio-Mazoyer N, Landeau B, Papathanassiou D, et al. Automated anatomical labeling of activations in SPM using a macroscopic anatomical parcellation of the MNI MRI single-subject brain. Neuroimage 2002;15:273–289.
19. Keuken MC, Bazin PL, Crown L, et al. Quantifying inter-individual anatomical variability in the subcortex using 7 T structural MRI. Neuroimage 2014;94:40–46.
20. Cselényi Z, Olsson H, Halldin C, Gulyás B, Farde L. A comparison of recent parametric neuroreceptor mapping approaches based on measurements with the high affinity PET radioligands [11C]FLB 457 and [11C]WAY 100635. Neuroimage 2006;32:1690–1708.
21. Tuisku J, Plavén-Sigray P, Gaiser EC, et al. Effects of age, BMI and sex on the glial cell marker TSPO - a multicentre [^{11}C]PBR28 HRRT PET study. Eur J Nucl Med Mol Imaging 2019;46:2329–2338.
22. Habeck C, Stern Y, Alzheimer's Disease Neuroimaging Initiative. Multivariate data analysis for neuroimaging data: overview and application to Alzheimer's disease. Cell Biochem Biophys 2010;58:53–67.
23. Benjamini Y, Hochberg Y. Controlling the false discovery rate: a practical and powerful approach to multiple testing. J R Stat Soc B 1995;57:289–300.
24. Cohen J. A coefficient of agreement for nominal scales. Educ Psychol Meas 1960;20:37–46.
25. Fleiss JL. Measuring nominal scale agreement among many raters. Psychol Bull 1971;76:378–382.
26. Nykjaer CH, Brudek T, Salvesen L, Pakkenberg B. Changes in the cell population in brain white matter in multiple system atrophy. Mov Disord 2017;3:1074–1082.
27. Cosenza-Nashat M, Zhao ML, Suh HS, et al. Expression of the translocator protein of 18 kDa by microglia, macrophages and astrocytes based on immunohistochemical localization in abnormal human brain. Neuropathol Appl Neurobiol 2009;35:306–328.
28. Lavisse S, Guillermier M, Hérard AS, et al. Reactive astrocytes overexpress TSPO and are detected by TSPO positron emission tomography imaging. J Neurosci 2012;32:10809–10818.
29. Hoffmann A, Ettle B, Battis K, et al. Oligodendroglial α-synucleinopathy-driven neuroinflammation in multiple system atrophy. Brain Pathol 2019;29:380–396.
30. Song YJ, Lundvig DM, Huang Y, et al. p25alpha relocalizes in oligodendroglia from myelin to cytoplasmic inclusions in multiple system atrophy. Am J Pathol 2007;71:1291–1303.
31. Valdinocci D, Radford RAW, Goulding M, Hayashi J, Chung RS, Pountney DL. Extracellular interactions of alpha-Synuclein in multiple system atrophy. Int J Mol Sci 2018;19:4129.
32. Tong J, Wong H, Guttman M, et al. Brain alpha-synuclein accumulation in multiple system atrophy, Parkinson's disease and progressive supranuclear palsy: a comparative investigation. Brain 2010; 133:172–188.
33. Lyoo CH, Ikawa M, Liow JS, et al. Cerebellum can serve as a pseudo-reference region in Alzheimer disease to detect Neuroinflammation measured with PET Radioligand binding to Translocator protein. J Nucl Med 2015;56:701–706.
34. Goebel G, Seppi K, Donnemiller E, et al. A novel computer-assisted image analysis of [123I]β-CIT SPECT images improves the diagnostic accuracy of parkinsonian disorders. Eur J Nucl Med Mol Imaging 2011;38:702–710.
35. Tang CC, Poston KL, Eckert T, et al. Differential diagnosis of parkinsonism: a metabolic imaging study using pattern analysis. Lancet Neurol 2010;9:149–158.
36. Archer DB, Bricker JT, Chu WT, et al. Development and validation of the automated imaging differentiation in parkinsonism (AID-P): a multisite machine learning study. Lancet Digit Health 2019;1:e222–e231.
37. Krismer F, Beliveau V, Seppi K, et al. Automated analysis of diffusion-weighted magnetic resonance imaging for the differential diagnosis of multiple system atrophy from Parkinson's disease. Mov Disord 2021;36:241–245.
38. Péran P, Barbagallo G, Nemmi F, et al. MRI supervised and unsupervised classification of Parkinson's disease and multiple system atrophy. Mov Disord 2018;33:600–608.
39. Vergnet S, Hives F, Foubert-Samier A, et al. Dopamine transporter imaging for the diagnosis of multiple system atrophy cerebellar type. Parkinsonism Relat Disord 2019;63:199–203.
40. Gu SC, Ye Q, Yuan CX. Metabolic pattern analysis of ^{18}F-FDG PET as a marker for Parkinson's disease: a systematic review and meta-analysis. Rev Neurosci 2019;30:743–756.
41. Jellinger KA, Seppi K, Wenning GK. Grading of neuropathology in multiple system atrophy: proposal for a novel scale. Mov Disord 2005;20(suppl 12):S29–S36.
42. Kreisl WC, Kim MJ, Coughlin JM, Henter ID, Owen DR, Innis RB. PET imaging of neuroinflammation in neurological disorders. Lancet Neurol 2020;19:940–950.

43. Gerhard A, Trender-Gerhard I, Turkheimer F, Quinn NP, Bhatia KP, Brooks DJ. In vivo imaging of microglial activation with [11C](R)-PK11195 PET in progressive supranuclear palsy. Mov Disord 2006;21:89–93.

44. Gerhard A, Watts J, Trender-Gerhard I, et al. In vivo imaging of microglial activation with [11C](R)-PK11195 PET in corticobasal degeneration. Mov Disord 2004;19:1221–1226.

45. Ghadery C, Koshimori Y, Coakeley S, et al. Microglial activation in Parkinson's disease using [^{18}F]-FEPPA. J Neuroinflammation 2017;14:8.

46. Koshimori Y, Ko JH, Mizrahi R, et al. Imaging striatal microglial activation in patients with Parkinson's disease. PLoS One 2015;10: e0138721.

47. Varnäs K, Cselényi Z, Jucaite A, et al. PET imaging of [^{11}C]PBR28 in Parkinson's disease patients does not indicate increased binding to TSPO despite reduced dopamine transporter binding. Eur J Nucl Med Mol Imaging 2019;46:367–375.

48. Ikawa M, Lohith TG, Shrestha S, et al. 11C-ER176, a Radioligand for 18-kDa Translocator protein, has adequate sensitivity to robustly image all three affinity genotypes in human brain. J Nucl Med 2017;58:320–325.

Supporting Data

Additional Supporting Information may be found in the online version of this article at the publisher's web-site.